

Electron-spectroscopy study of rare-earth trihalides

K.-H. Park and S.-J. Oh

Department of Physics, Seoul National University, Seoul 151-742, Korea

(Received 3 June 1993)

We have studied the electronic structures of rare-earth trihalides LaF_3 , LaCl_3 , CeF_3 , CeCl_3 , and GdF_3 by x-ray photoemission spectroscopy (XPS), bremsstrahlung isochromat spectroscopy (BIS), and electron-energy-loss spectroscopy (EELS). The double peak structures of the rare-earth $3d$ core-level XPS can be understood within the Anderson impurity model as being due to the charge transfer from the ligand $2p$ level to the rare-earth unfilled $4f$ level. The parameters obtained from fitting these core-level spectra using the Gunnarsson-Schönhammer-model approach are consistent with the valence-band XPS and the conduction-band BIS spectra. In the higher binding-energy side (10–40 eV) of $3d$ XPS, several more satellites are observed. Through comparing with other core-level XPS and EELS, we find that they are mainly loss structures arising from the interband transition, the rare-earth $5p$ excitation, and the charge-transfer transition, but there are some contributions from the “intrinsic” plasmon excitations as well.

I. INTRODUCTION

Rare-earth compounds show interesting physical properties such as mixed valency, heavy fermion, and Kondo-like behaviors due to the interaction between the localized $4f$ electrons and the delocalized conduction bands. Their electronic structures have been extensively studied by electron spectroscopic techniques^{1–5} such as photoelectron spectroscopy (PES), bremsstrahlung isochromat spectroscopy (BIS), and electron-energy-loss spectroscopy (EELS), and these studies were very useful in elucidating the physical origin of their interesting properties. In particular, it has been shown¹ that valence-band PES, core-level x-ray photoemission spectroscopy (XPS), and conduction-band BIS spectra can be interpreted consistently within the Gunnarsson-Schönhammer (GS) model² of the Anderson impurity Hamiltonian, and that the parameters obtained from fitting these high-energy spectroscopy data can be used to predict the low-energy measurement data such as the magnetic susceptibility, which usually show good agreement with the experiments.

However, until now these studies have been mainly performed on the metallic rare-earth compounds, and the comprehensive electron spectroscopic studies on the insulating rare-earth compounds are relatively few. In this paper, we report such comprehensive electron spectroscopic studies on the insulating rare-earth trihalides LaF_3 , LaCl_3 , CeF_3 , CeCl_3 , and GdF_3 using the valence-band and core-level XPS, BIS, and EELS techniques. These trihalides are wide band-gap insulators, and the rare-earth ions in these compounds are expected to be in the trivalent state. It would be interesting to see how well the Gunnarsson-Schönhammer model can explain these electron-spectroscopy data consistently, and how the parameter values of the Anderson impurity Hamiltonian such as the hybridization strength and the Coulomb correlation energies for these insulators compare with those for the metallic compounds.

Particularly interesting are the double peak structures

seen in the rare-earth $3d$ core-level spectra of lanthanum and cerium trihalides,^{6–9} where the intensity ratio between the two peaks shows dramatic change depending on the halide element. Similar double peak structures are well known in the $4f$ photoemission spectra of many rare-earth compounds, which have been the subject of intensive studies^{1–5} in recent years. Two different models have been proposed for the origin of these double peak structures. In the framework of the Gunnarsson-Schönhammer model, these double peaks are described by two final states with different f -level occupancies, and the peak near the Fermi level is related to the Kondo resonance. But another screening model by conduction $5d$ electrons was suggested by Liu and Ho.³ In this $5d$ screening model, the $5d$ impurity bound state is created by Coulomb interaction between the $4f$ hole and the $5d$ electron, and the fully screened peak by the occupation of this $5d$ bound state appears at the Fermi level, while the poorly screened peak with empty $5d$ bound state appears at a few eV higher binding energy. For the insulating rare-earth trihalide compounds, Fujimori *et al.*¹⁰ performed a resonant photoemission study and found that their $4f$ spectra also show similar a double peak structure. They therefore concluded that the $5d$ screening model is not relevant for the double peak structure since the $5d$ states are empty in these trihalides. They also showed that the intensity ratio and the energy separation between two $4f$ peaks of these compounds are well described by the cluster model,⁸ which is similar to the GS model in describing the photoemission spectra of the insulating rare-earth compounds, except that the ligand valence band is simplified as a discrete level. It would be interesting to see whether the double peak structures seen in the rare-earth $3d$ core-level spectra of these trihalides can also be described by the GS model, with parameter values consistent with the valence-band $4f$ XPS and BIS spectra.

In the $3d$ core-level XPS, additional structures at 10–40-eV higher binding energy of the main peak are ob-

served. Structures at this binding-energy range have also been reported in the $3d$ core-level spectra of other compounds,¹ and ascribed to various origins. In the mixed valence Ce compounds like α -Ce metal and CeNi_x ,¹ they arise from the initial f^0 configuration mixing, and similar high binding-energy satellites show up in the insulating tetravalent cerium compounds like CeO_2 (Refs. 4 and 11) and CeF_4 (Ref. 12) due to the initial covalency mixing of the f^0 configuration. For the semimetallic Ce pnictide compounds, Takeshige, Sakai, and Kasuya¹³ proposed structures at this binding-energy range due to the intrinsic p - d antibonding state, which arise from the hybridization effect between the valence-band electrons and the cation $5d$ electrons. And of course loss structures such as plasmon excitation peaks can appear at this energy range. In order to understand the origin of these higher binding-energy structures seen in the $3d$ core-level spectra, we performed EELS experiments with various incident electron energies (300–1500 eV). In this way we could distinguish between the “extrinsic” loss structures and the “intrinsic” satellites, and by comparing with valence band XPS and BIS spectra, the origin of various loss structures could be identified.

The organization of this paper is as follows. In Sec. II the experimental details are described. In Sec. III we present and interpret the experimental results, and discuss their implications. The paper concludes with the summary in Sec. IV.

II. EXPERIMENT

All the XPS, BIS, and EELS spectra were taken from evaporated thin films. Powder samples of LaF_3 , LaCl_3 , CeF_3 , CeCl_3 , and GdF_3 with purity 99.99% were commercially obtained from the Johnson & Matthey Co., and thermally evaporated onto the stainless-steel sample holder with the thickness of a few tens of Å. By this method we were able to obtain clean sample surfaces, and could avoid the problem of the binding-energy shift due to the sample charging effect of these good insulating samples. We could also avoid local heating, which can severely damage the sample surfaces during BIS and EELS experiments. In the course of XPS, EELS, and BIS experiments the pressure of the spectrometer were kept below 6×10^{-10} Torr. Our analyzer system is the concentric hemispherical analyzer (CHA) made by VSW Scientific Instrument Ltd., and the constant analysis energy mode was used with the pass energy of 22 eV for XPS and EELS. In XPS the photon source was $\text{Mg } K\alpha$ ($h\nu=1253.6$ eV), which gave the total instrumental resolution (full width at half maximum) including the photon and analyzer broadenings of 0.9 eV. For the BIS measurement a x-ray monochromator with a transmission energy of 1486.6 eV was used. The energy spread of the electron gun for BIS was 0.8 eV, resulting in a total BIS resolution of 0.85 eV. The typical sample current from the e gun during the BIS measurement was 20–30 μA . The same gun was used for the EELS experiment with a typical sample current of 1–2 μA , which gave a similar incident electron energy spread. Reflection mode geometry was used for the EELS experiment.

III. RESULT AND DISCUSSION

A. Valence-band XPS and BIS spectra

In Fig. 1, the valence XPS and BIS spectra of all trihalide samples studied here are shown. In the case of lanthanum trihalides the valence bands are composed of only F $2p$ or Cl $3p$ states as shown in Fig. 1(a), since no $4f$ level is occupied. But in cerium trihalides shown in Fig. 1(b), we expect the Ce $4f$ level also contributes to the valence-band spectra. By comparing these two spectra, we can deduce that the Ce $4f$ level gives a distinct peak at a binding energy of ~ 4 eV in CeF_3 , while it is mixed with Cl $3p$ structures in CeCl_3 . These findings are consistent with the conclusions of Fujimori *et al.*,¹⁰ who extracted the Ce $4f$ emission using the resonance photoemission technique at the Ce $4d$ absorption edge. In the case of GdF_3 [Fig. 1(c)], the $4f^7 \rightarrow 4f^6$ emission, which is strong because of the large number of $4f$ electrons, overlaps in energy with the F $2p$ emissions. The BIS spectra for all the compounds are dominated by the $4f^n \rightarrow 4f^{n+1}$ transition due to their large cross sections, where $n=0, 1$, and 7 for La, Ce, and Gd trihalides, respectively.

From the combination of the valence-band XPS and BIS spectra, we can obtain values of various parameters in the Anderson Hamiltonian for these compounds. Table I lists the energy positions of various features in Fig. 1 relative to the Fermi level. For the position of the Ce $4f$ emission in CeCl_3 , which is difficult to separate from the Cl $3p$ emissions in our XPS spectra, we used the resonant photoemission data of Ref. 10. The charge-transfer energy Δ is defined as the energy required to take an electron from the ligand p level to the unoccupied rare-earth $4f$ level, which we find from this table to be 14–15 eV for fluorides and 9–10 eV for chlorides regardless of cation rare-earth atoms. The intra-atomic $4f$ correlation energies U_{ff} can also be obtained from the energy separations between the $4f^n \rightarrow 4f^{n-1}$ transition in XPS and the $4f^n \rightarrow 4f^{n+1}$ transition in BIS. In Fig. 1 we can also see the rare-earth $5s$, $5p_{3/2}$, and $5p_{1/2}$ peaks, whose binding energies are listed in Table I. These shallow core-level energies are needed for the discussion of energy-loss structures that follows.

B. Double peak structures of rare-earth $3d$ spectra

In Fig. 2, the XPS spectra of the rare-earth $3d$ core-level region are shown. In the spectra of La and Ce trihalides, the double peak structures for each spin-orbit pair $3d_{3/2}$ and $3d_{5/2}$ are apparent, as reported earlier.^{6–9} In addition, weak satellites in the far side of the main peak (10–40-eV higher binding energy) can be seen. We will discuss only the near-side double peak structures in this section, and defer the discussion on the weak higher binding-energy satellites to Sec. III C.

The double peak structures of rare-earth $3d$ core-level spectra in many rare-earth compounds have been understood in terms of the Anderson impurity Hamiltonian.^{1,2,9} The Anderson impurity Hamiltonian for the description of the core-level spectra is given by

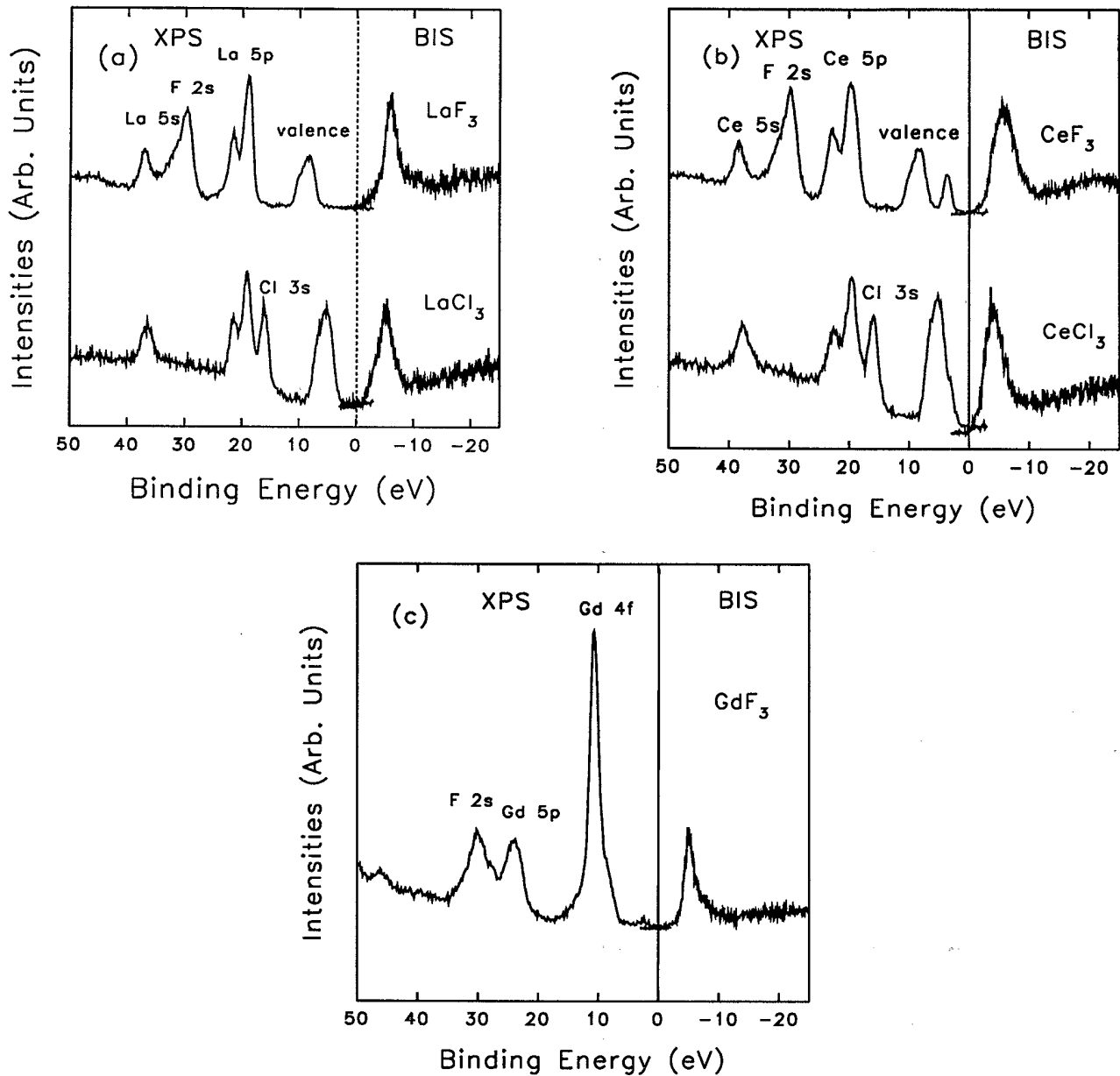


FIG. 1. The valence-band XPS and BIS spectra of (a) LaF_3 and LaCl_3 , (b) CeF_3 and CeCl_3 , and (c) GdF_3 . The vertical scales between XPS and BIS spectra are arbitrary, and the binding-energy reference is the Fermi level.

TABLE I. Binding energies relative to the Fermi level in the valence-band XPS and the unoccupied $4f$ level energy in BIS (in units of eV; RE stands for the rare-earth element). The binding energy of the $\text{Gd } 5p_{1/2}$ peak cannot be determined unambiguously due to the overlap with the $\text{F } 2s$ peak.

Compounds	F $2p$	RE $4f$	RE $5p_{3/2}$	RE $5p_{1/2}$	RE $5s$	RE $4f$ (BIS)
LaF_3	8.8		18.9	21.6	37.1	6.0
CeF_3	8.8	3.7	19.7	22.8	38.3	5.6
GdF_3	8.8	10.6	24.0			5.2
	Cl $3p$	RE $4f$	RE $5p_{3/2}$	RE $5p_{1/2}$	RE $5s$	RE $4f$ (BIS)
LaCl_3	5.6		19.1	21.5	36.5	5.1
CeCl_3	5.5		19.7	22.6	37.8	4.2

$$\begin{aligned}
 H = & \sum_{\mu=1}^{N_f} \left[\varepsilon_f \hat{\Psi}_{\mu}^{\dagger} \hat{\Psi}_{\mu} + \int d\varepsilon \varepsilon \hat{\Psi}_{\mu\varepsilon}^{\dagger} \hat{\Psi}_{\mu\varepsilon} - Q(1-n_c) \hat{\Psi}_{\mu}^{\dagger} \hat{\Psi}_{\mu} \right] \\
 & + \sum_{\mu=1}^{N_f} \left[\int d\varepsilon V(\varepsilon) \hat{\Psi}_{\mu}^{\dagger} \hat{\Psi}_{\mu\varepsilon} + \text{H.c.} \right] \\
 & + U_{ff} \sum_{\mu < \nu}^{N_f} n_{\mu} n_{\nu} + \varepsilon_c \hat{\Psi}_c^{\dagger} \hat{\Psi}_c, \quad (1)
 \end{aligned}$$

where V is the hybridization between $4f$ and conduction-band states, U_{ff} is the correlation energy between $4f$ electrons, and Q is the core-hole $4f$ electron Coulomb attraction energy.

Using the configurations $|f^n\rangle$, $|f^{n+1}\underline{v}(\varepsilon)\rangle$, $|f^{n+2}\underline{v}^2(\varepsilon, \varepsilon)\rangle$, and $|f^{n+2}\underline{v}^2(\varepsilon, \varepsilon')\rangle$ as basis states, we can

obtain the initial and final Hamiltonian matrix components, and the core XPS spectrum at zero temperature is given by

$$\rho_c(\varepsilon) = \frac{1}{\pi} \text{Im}g(\varepsilon - i0^+) \quad (2)$$

where $g(z) = \langle \Phi_0 | \hat{\psi}_c^{\dagger} \{ 1/[z - E_0(N) + H] \} \hat{\psi}_c | \Phi_0 \rangle$ for the ground state $|\Phi_0\rangle$. In our model calculation, we divided the ligand valence band to 20 discrete levels, and assumed that the hybridization strength has the following semi-elliptical form:

$$[V(\varepsilon)]^2 = 2V^2 \sqrt{B^2 - \varepsilon^2} / \pi B^2, \quad (3)$$

where $2B$ is the width of the valence band.

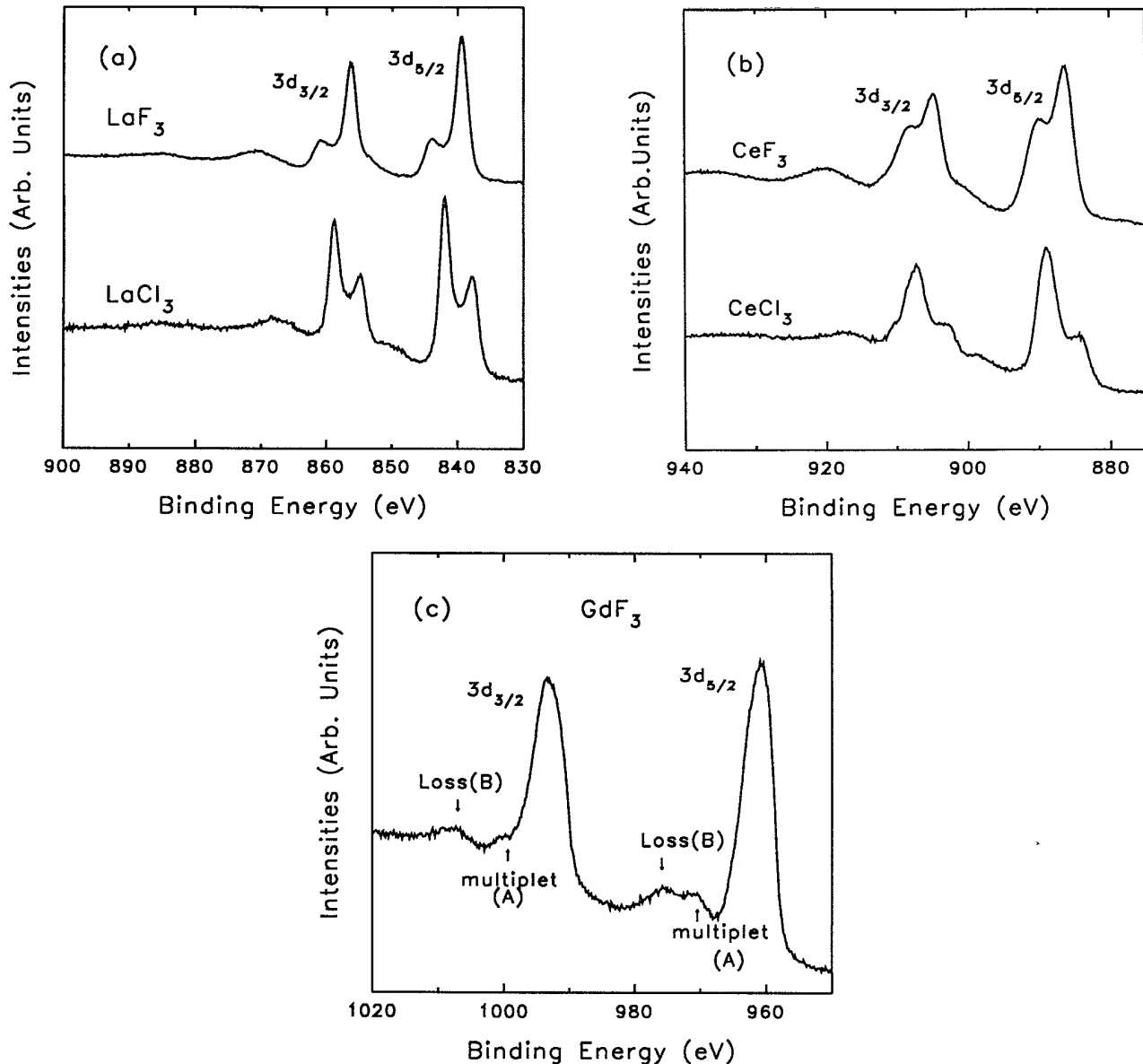


FIG. 2. Wide view of the rare-earth $3d$ core-level XPS spectra of (a) LaF_3 and LaCl_3 , (b) CeF_3 and CeCl_3 , and (c) GdF_3 . We can see the double-peak structures in the lower binding-energy region, and weak high binding-energy satellites.

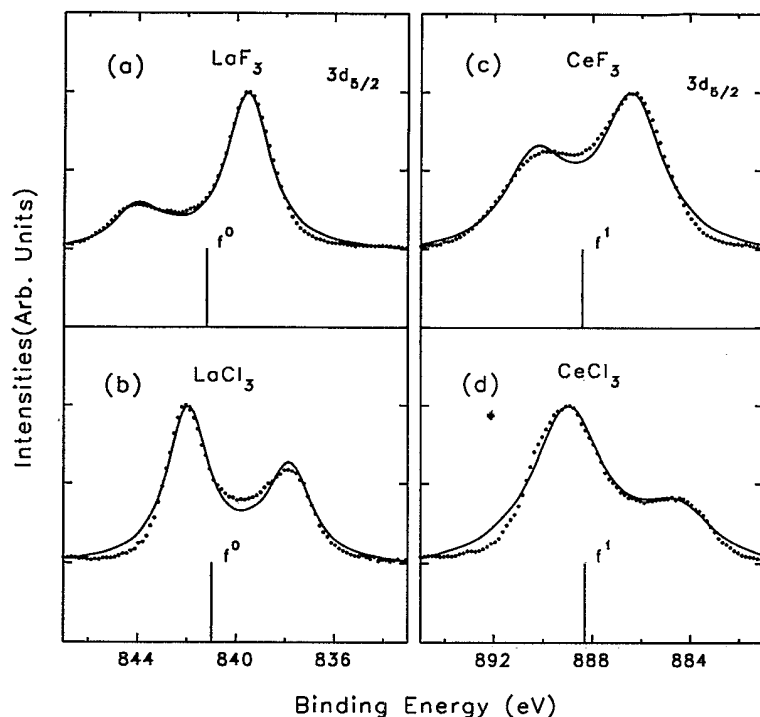


FIG. 3. Double peaks of the experimental $3d_{5/2}$ spectra (points) and theoretical curves (lines) from the GS model for (a) LaF_3 , (b) LaCl_3 , (c) CeF_3 , and (d) CeCl_3 . The vertical lines denote the binding-energy positions of the pure $3d_{5/2}f^n$ configuration in the GS model calculation.

In the model fitting of our rare-earth $3d$ spectra using this Hamiltonian, we tried to use parameter values deduced from the XPS/BIS spectra shown in Fig. 1. First, the charge-transfer energy Δ , which is determined by the relative energy position of the rare-earth $4f$ level and the ligand p level, has been obtained from Table I. And the $4f$ electron correlation energy U_{ff} for Ce compounds has also been taken from Table I. In the case of LaF_3 , the value of U_{ff} was borrowed from previous papers,^{14,15} and the same value was used for the LaCl_3 case although it may not be a good approximation. The only free parameters in our fitting were the hybridization strength V and the Coulomb attraction energy Q between the $4f$ electron and the core hole, and we varied these values to get the best agreements between the experimental spectra and the theoretical curve for each compound.

In Fig. 3, we show the results of our model fitting for La and Ce trifluorides and trichlorides, and the parameter values for the best fit are given in Table II. We see that the theory curves fit the experimental spectra very well, both in terms of the energy positions and the intensity ratios. The parameter values shown in Table II are also very reasonable. The hybridization parameter of the La trihalide is larger than that of the Ce trihalide, and the value of Q is larger in Ce compounds than in La compounds. Both trends are expected from the lanthanide contraction, since the $4f$ wave function shrinks at higher atomic number when there are more positive nuclear charges. We also find that for a given rare-earth ion, the value of Q is larger in fluoride than in chloride. This can be understood by the difference of screening by valence electrons, which is more effective in more covalent chlorides than very ionic fluorides. Also the value of $\epsilon_{3d_{5/2}}^0$, which is the bare binding energy of the $3d_{5/2}f^n$

configuration (underline denotes a hole) in the GS model calculation, is shown to be almost the same for a given rare-earth element regardless of the halide ligand. This should be the case if we can neglect the chemical shift phenomenon, since $\epsilon_{3d_{5/2}}^0$ is an atomic quantity. For some of the compounds studied here, similar parameter values were obtained earlier from the cluster model calculation^{8,10} or the Anderson impurity model calculation.^{9,15} However, our values are more consistent in that (i) the values of Δ and U_{ff} are determined *a priori* from the XPS and BIS spectra rather than taken as free fitting parameters; (ii) some inconsistency of earlier parameter values, such as a larger Q value for La than Ce compounds,⁹ is now removed; and (iii) the absolute binding energy as well

TABLE II. Parameter values in the curve fitting of the rare-earth $3d_{5/2}$ spectra using the GS model. Here the meanings of the symbols are as follows. ϵ_{3d}^0 : pure $3d f^n$ configuration binding energy in the GS model calculation; Δ : the charge-transfer energy from the ligand level to the unoccupied rare-earth $4f$ level determined by the valence XPS and BIS; Q : core-hole $4f$ Coulomb attraction energy; V : hybridization value between the $4f$ level and the valence band; U_{ff} : the $4f$ correlation energy obtained from the $4f$ binding energy in XPS and the unoccupied $4f$ level energy in BIS; B : half-width of the valence band; and n : the number of occupied $4f$ levels, $n=0$ for La, and 1 for Ce compounds. Units are eV.

Compounds	$\epsilon_{3d_{5/2}}^0$	Δ	Q	$\Delta - Q$	$\sqrt{N_f - n} V$	U_{ff}	B
LaF_3	841.2	14.8	12.7	2.1	2.2	8.0	1.0
LaCl_3	841.0	10.7	12.0	-1.3	1.9	8.0	1.0
CeF_3	888.4	14.4	13.8	0.6	2.1	9.3	1.0
CeCl_3	888.3	9.7	12.2	-2.5	1.6	7.3	1.0

as the $\epsilon_{3d_{5/2}}^0$ value can be determined because we avoided the charging problem by using evaporated thin-film samples.

In the double peak structures shown in Fig. 3, the lower binding-energy peaks are stronger in LaF_3 and CeF_3 , but the higher binding-energy peaks are stronger in LaCl_3 and CeCl_3 . This change of the relative intensity is naturally understood within the charge-transfer model as follows. The photoemission peak intensity under the sudden approximation is proportional to the square of the overlap of the wave functions between the initial ground state and the final eigenstates. For the trihalides studied here the charge-transfer energy Δ is much larger than the hybridization strength, and therefore in the initial state the ground configuration is nearly f^n in both fluorides and chlorides. But in the final-state Hamiltonian the charge-transfer energy is reduced to $\Delta - Q$, and so the energy ordering between f^n and f^{n+1} configurations is reversed between fluoride and chloride, as shown in Table II. Hence in fluorides the low binding-energy peak is mainly composed of the f^n configuration, whereas in chlorides the f^{n+1} is the major component of the low binding-energy peak. This gives rise to the reversal of the intensity between two peaks. A similar idea has been discussed for the case of lanthanum halides within the Anderson impurity model calculation.¹⁵

In the XPS spectra of shallow rare-earth core levels such as $5s$ and $5p$ shown in Fig. 1 of Sec. III A, we find that only a single peak appears, unlike the $3d$ spectra discussed here. The reason is that the Coulomb attraction energy between, say, the $5s$ core hole and the $4f$ electron Q_{5s} is much smaller than that of the $3d$ hole Q_{3d} . To estimate the value of Q_{5s} , we calculated the $4f$ ionization energies of the Ce $3+$ ion in the presence of the $3s$ and

the $5s$ core holes using the atomic Hartree-Fock (HF) program. We assumed that the difference of these two energies, $E_{4f}(3s) - E_{4f}(5s)$, is the same as the difference of the core-hole attraction energies $Q_{3d} - Q_{5s}$. (We used the $3s$ hole instead of the $3d$ hole in the atomic HF calculation to avoid the ambiguity due to the multiplet structure of the $3d4f$ configuration.) This is probably not a bad approximation since the $3s$ and the $3d$ core holes belong to the same principal quantum number, so that the relaxation of the outer electrons would be almost the same. We find that $E_{4f}(3s) - E_{4f}(5s) = 7.94$ eV in Ce^{3+} , so the Coulomb attraction energy Q_{5s} is estimated to be around 4 eV using the Q_{3d} value of 12–13 eV shown in Table II. When we calculate the $5s$ GS theoretical spectra for this value of small Q ($Q_{5s} = 4$ eV), we indeed obtain only a single peak consistent with the experiments.

In the Gd $3d$ spectra of GdF_3 shown in Fig. 2(c), we also see two "satellites" A and B corresponding to each spin-orbit peak. We believe that peaks A and A' arise from the multiplet structures of $3d_{5/2}4f^7$ and $3d_{3/2}4f^7$ configurations, respectively, judging from their energy positions and intensity ratios compared with the theoretical calculation of the multiplet structure of the $3d$ core-level spectra on Gd metal.¹⁶ Peaks B and B' are probably loss structures from the charge-transfer transition, as will be discussed in Sec. III C. These interpretations are consistent with the expectation that the charge-transfer satellites such as occur in Ce and La compounds would be small in GdF_3 because of the small hybridization value.

C. Higher binding-energy satellites

As mentioned earlier, there are weak satellites in the higher-binding energy side of the rare-earth $3d$ core level

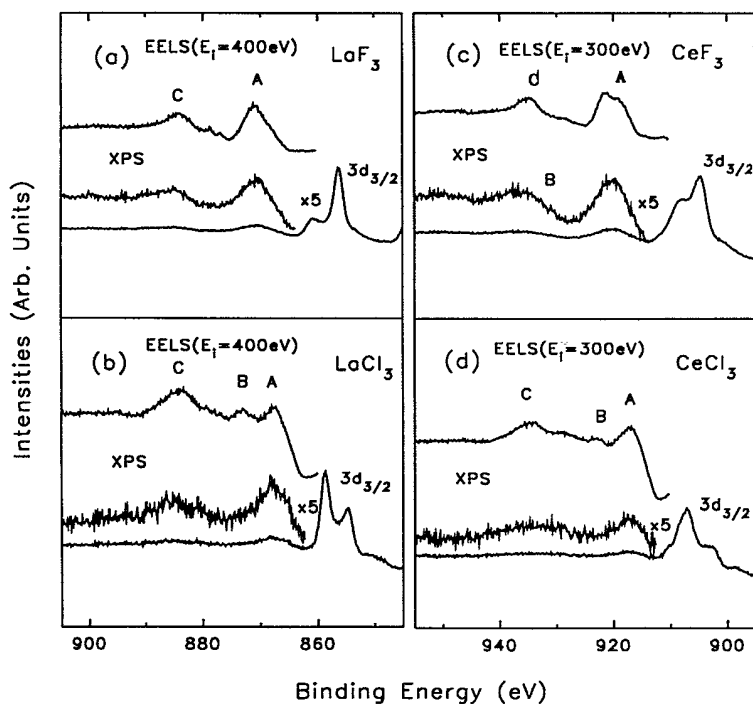


FIG. 4. Higher-binding-energy-side satellites of the rare-earth $3d_{3/2}$ XPS spectra compared with the EELS for (a) LaF_3 , (b) LaCl_3 , (c) CeF_3 , and (d) CeCl_3 . Peak A is assigned as the charge-transfer transition loss peak, B is the plasmon loss peak, and C is the $5p$ transition loss peak. The XPS satellites are magnified by five times in vertical scale to show the peaks clearly. The source energies in EELS are chosen to have similar kinetic energies to the specific XPS core level.

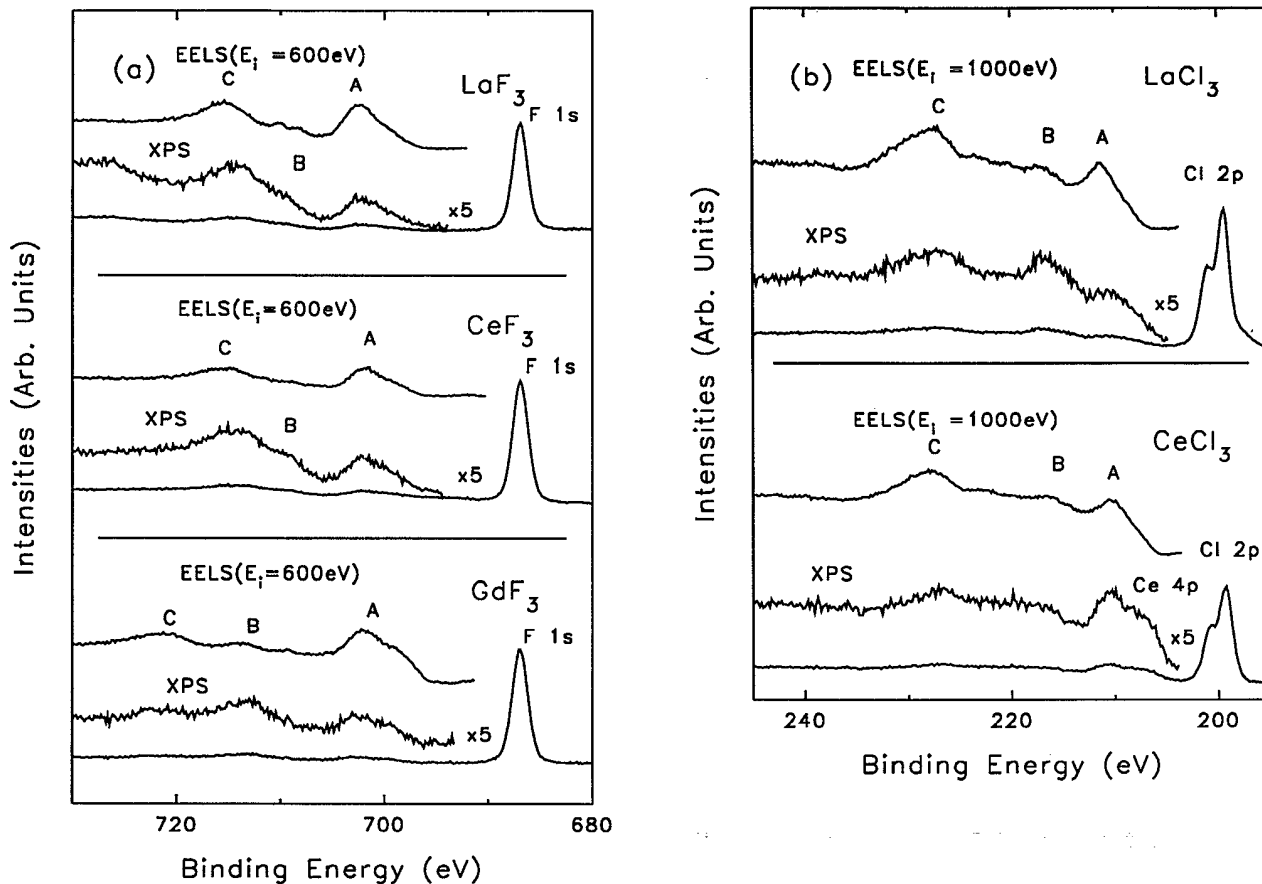


FIG. 5. Higher-binding-energy-side satellites of anion F 1s and Cl 2p core levels, and the EELS loss spectra for (a) LaF_3 , CeF_3 , and GdF_3 , and (b) LaCl_3 and CeCl_3 . The XPS satellites are magnified five times in vertical scale to show the peaks clearly. The source energies in EELS are chosen to have similar kinetic energies to the specific XPS core level.

in addition to the double peak structures analyzed above. In Figs. 4 and 5 we show a detailed scan of the higher binding-energy regions of the rare-earth $3d_{3/2}$ core-level and anion core-level XPS spectra. Their rich features need careful analysis. In order to extract the "extrinsic" loss structures which arise from various excitations dur-

ing the transport of high kinetic-energy photoelectrons through the solid to the surface, we measured EELS spectra with incident electrons of about the same kinetic energy as XPS core-level photoelectrons. We find that these higher binding-energy satellites of core-level XPS resemble the loss spectra of EELS except that the relative in-

TABLE III. The energies of three loss peaks in EELS and XPS relative to the incident energy or the anion main peak. The EELS incident electron energy was 600 eV for LaF_3 , CeF_3 , and GdF_3 , and 1000 eV for LaCl_3 and CeCl_3 . The expected plasmon energy calculated by the nearly-free-electron approximation is also shown for each compound. Units are eV.

Compounds	Spectroscopy	$E_{\text{Loss}}(A)$	$E_{\text{Loss}}(B)$	$E_{\text{Loss}}(C)$	$E_{\text{plasmon}}(\text{NFA})$
LaF_3	EELS	14.8		28.7	
	Anion XPS	14.9		27.1	
LaCl_3	EELS	10.5	16.5	27.4	15.4
	Anion XPS	10.4	16.8	27.6	
CeF_3	EELS	14.6	22.7	29.0	21.7
	Anion XPS	14.4	22.7	27.6	
CeCl_3	EELS	10.0	16.3	28.1	15.5
	Anion XPS	14.9	26.3	35.0	

tensities of various peaks are somewhat different. [In the Cl $2p$ spectra of $CeCl_3$ shown in Fig. 5(b), Ce $4p$ peaks are mixed.] This suggests that most of these weak satellites are extrinsic loss structures.

To understand the origin of these satellites, in Table III we list the centroid energy positions of three peaks A , B , and C relative to the main peak in the XPS spectra, or

the amount of the energy loss in the EELS spectra. We find that the loss energy of peak A is 14–15 eV in fluoride compounds, and 10–11 eV in chlorides, which are very close to the charge-transfer energies Δ shown in Table II. Hence, the first loss peak A in EELS is considered to be the charge-transfer loss peak. This charge-transfer loss peak is composed of the interband transition

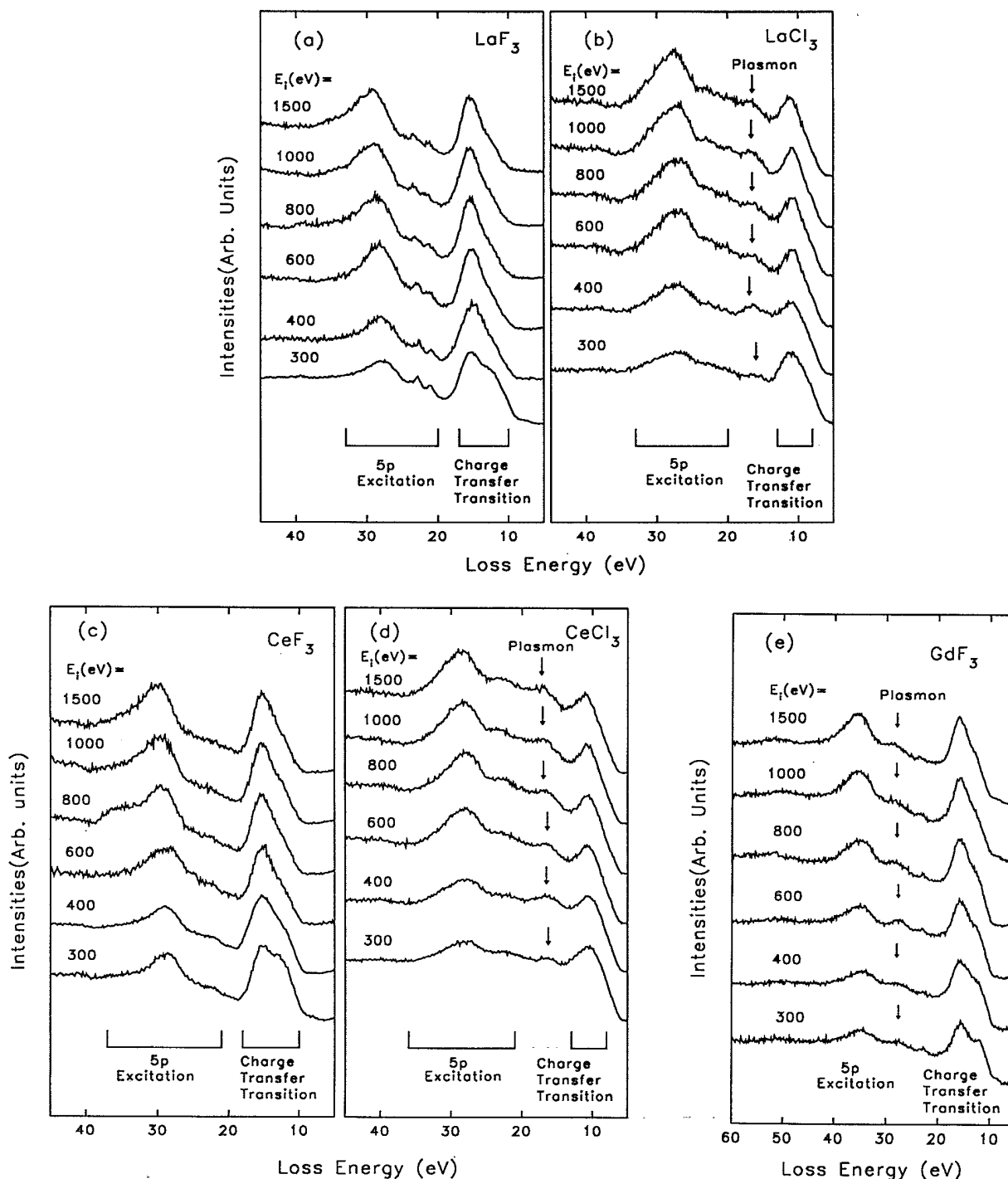


FIG. 6. The EELS loss spectra with various incident kinetic energies between 300 and 1500 eV for (a) LaF_3 , (b) $LaCl_3$, (c) CeF_3 , (d) $CeCl_3$, and (e) GdF_3 . The peaks indicated with arrows are the plasmon loss peaks.

channels from the ligand valence band to the rare-earth $4f$, $5d$, and $6s$ conduction bands. Similar interband transition channels of rare-earth fluoride compounds were observed before by Olson, Piacentini, and Lynch¹⁷ in optical reflectance spectra, where strong reflectance peaks by interband absorption appear in the 10–15-eV region. In our case the broad interband transition peaks from the valence band to the $5d$ and $6s$ conduction bands and a sharp interband transition peak from the valence band to the unoccupied $4f$ level would be mixed. The loss peaks “C” between 25 and ~40 eV are certainly due to the excitations from the rare-earth $5p$ to the conduction band, since their energies depend on the rare-earth $5p$ binding energy and are very close to the $5p_{1/2} \rightarrow 4f$ transition energies shown in Table I. These $5p$ excitation satellites have been reported before in several rare-earth compounds.^{18,19}

The loss structure “B” can be assigned as the plasmon loss peak judging from its energy. The plasmon energy in the free-electron approximation is given by the equation

$$\omega_p^2 = 4\pi n e^2 / m, \quad (4)$$

where m is the mass of the free electron, and n is the density of valence electrons. This equation has been used to calculate the plasmon energy in metallic and semiconducting materials.^{20,21} Even for many insulating compounds, it was recently shown²² that this equation predicts the plasmon energy very well if only the delocalized valence electrons are included for the electron density n . Thus we use this equation in order to calculate the plasmon energy for the insulating trihalide compounds studied here with the free-electron mass m and the value of n assuming 18 electrons per RH_3 cluster (R : rare earth; H : halide element) with the known lattice constants.²³ In Table III, the plasmon energies thus calculated are compared with the “B” loss energy, and the obvious correspondences can be seen. Interestingly we can see in Fig. 5 that the intensities of the B satellites in F $1s$ and Cl $2p$ XPS spectra are significantly larger than corresponding loss peaks in the EELS spectra with the same kinetic energy. This suggests that there is a significant contribution from the “intrinsic” plasmons in the core-level XPS spectra in addition to the “extrinsic” plasmons. On the other hand, in the rare-earth $3d_{3/2}$ core-level spectra of LaCl_3 and CeCl_3 shown in Fig. 4, the plasmon “B” loss peak seems weaker in XPS than in EELS. The reason for this apparent difference between anion and cation core-level XPS spectra is that the loss structure from the $3d_{5/2}$ main peak would be overlapped in the “A” loss region of the $3d_{3/2}$ peak in rare-earth XPS, and an interference effect exists between “intrinsic” and “extrinsic” plasmons in the small kinetic-energy regions of XPS.^{24,25}

D. Electron-energy-loss spectra

In Fig. 6, we show the electron-energy-loss spectra from rare-earth trihalides with incident electrons of various kinetic energies between 300 and 1500 eV. In EELS with high-energy electrons, the loss structure represents $\text{Im}(-1/\epsilon)$, where ϵ is the dielectric constant of the sam-

ple. Usually in metallic samples the EELS spectra show the plasmon loss and the interband transition structures. The loss peaks in rare-earth trihalide shown in Fig. 6 can be interpreted in a similar way. As discussed above, these loss structures consist mainly of three features: the first is the charge-transfer transition from the valence band to the unoccupied $4f$, $5d$, and $6s$ states, the second is the plasmon loss peak, and the third is the atomic $5p$ excitation. The plasmon loss peaks are not well resolved in LaF_3 and CeF_3 , where plasmon loss peaks overlap with larger $5p$ excitation structures.

It is interesting to note that in all trihalides studied here the intensity of the $5p$ excitation loss peak relative to that of the charge-transfer transition peak becomes larger as the incident electron energy becomes higher. Since the importance of the dipole transition increases at higher incident energy in EELS, this probably means that the $5p$ excitation is mainly the $5p \rightarrow 5d$ and $6s$ dipole transition, while the charge-transfer transition structure includes a considerable amount of nondipole transitions and surface plasmons. In Fig. 6 we can also see the tendency for the loss peak position to shift to a higher energy as the source energy becomes higher. This again can be interpreted as being due to the increasing importance of the dipole transition, implying that the empty $5d$ and $6s$ states are at higher energy than the empty $4f$ state.

In the EELS spectra of LaF_3 shown in Fig. 6(a), small sharp structures can be seen in the 20–25-eV loss region, whereas such sharp structures do not show up in other samples. Similar results were reported by Olson, Piacentini, and Lynch¹⁷ in their optical measurements. They suggested that these 20–25-eV structures are due to the $5p \rightarrow 5d$ and $6s$ atomic absorptions including crystal-field effects. Similar analysis could be applied to these sharp loss peak of our EELS spectra.

IV. SUMMARY

We obtained various core levels and the valence-band XPS of the insulating rare-earth trihalide compounds. In the $3d$ core-level XPS spectra of these compounds, the double peak structures and additional higher binding-energy satellites were observed. By applying the Gunnarsson-Schönhammer model of the Anderson impurity Hamiltonian, we can understand the details of double peak structures in a systematic way. The parameter values obtained from the fit, such as the charge-transfer energy, $4f$ electron correlation energy, and the hybridization strength, are all consistent with the valence-band XPS and BIS spectra and the expected trends. The higher binding-energy satellites in the $3d$ spectra are attributed to (1) charge-transfer excitation loss from the ligand valence band to the rare-earth $4f$, $5d$, and $6s$ levels, (2) rare-earth $5p$ excitation to $5d$ and $6s$ levels, and (3) collective plasmon loss whose intensity is different in XPS and in EELS due to the intrinsic process.

ACKNOWLEDGMENT

This work was supported by a grant from the Korean Science and Engineering Foundation.

- ¹J. W. Allen, S.-J. Oh, O. Gunnarsson, K. Schönhammer, M. B. Maple, M. S. Torikachvili, and I. Lindau, *Adv. Phys.* **35**, 275 (1986).
- ²O. Gunnarsson and K. Schönhammer, *Phys. Rev. Lett.* **50**, 604 (1983); *Phys. Rev. B* **28**, 4315 (1983); **31**, 4815 (1985).
- ³S.-H. Liu and K. M. Ho, *Phys. Rev. B* **26**, 7052 (1982); **28**, 4220 (1983).
- ⁴E. Wuilloud, B. Delly, W.-D. Schneider, and Y. Baer, *Phys. Rev. Lett.* **53**, 202 (1984).
- ⁵N. E. Bickers, D. L. Cox, and J. W. Wilkins, *Phys. Rev. Lett.* **54**, 23 (1985).
- ⁶A. J. Signorelli and R. G. Heyes, *Phys. Rev. B* **8**, 81 (1973).
- ⁷S. Suzuki, T. Ishii, and T. Sagawa, *J. Phys. Soc. Jpn.* **37**, 1334 (1974).
- ⁸A. Fujimori, *Phys. Rev. B* **27**, 3992 (1983).
- ⁹S. Imada and T. Jo, *Phys. Scr.* **41**, 115 (1990); *J. Phys. Soc. Jpn.* **58**, 402 (1989); **58**, 2665 (1989).
- ¹⁰A. Fujimori, T. Miyahara, T. Koide, T. Shidara, H. Kato, H. Fukutani, and S. Sato, *Phys. Rev. B* **38**, 7789 (1988).
- ¹¹A. Fujimori, *Phys. Rev. B* **28**, 2881 (1983).
- ¹²G. Kaindle, G. K. Wertheim, G. Schmiester, and E. V. Sampathkumaran, *Phys. Rev. Lett.* **58**, 606 (1987).
- ¹³M. Takeshige, O. Sakai, and T. Kasuya, *J. Phys. Soc. Jpn.* **60**, 666 (1991).
- ¹⁴S.-J. Oh, G.-H. Kim, G. A. Sawatzky, and H. T. Jonkman, *Phys. Rev. B* **37**, 6145 (1988).
- ¹⁵W.-D. Schneider, B. Delly, E. Wuilloud, J.-M. Imer, and Y. Baer, *Phys. Rev. B* **32**, 6819 (1985).
- ¹⁶S. Imada, *Physica B* (to be published).
- ¹⁷C. G. Olson, M. Piacentini, and D. W. Lynch, *Phys. Rev. B* **18**, 5740 (1978).
- ¹⁸F. P. Netzer, G. Strasser, G. Rosina, and J. A. D. Matthew, *Surf. Sci.* **152/153**, 757 (1985).
- ¹⁹A. Tonomura, J. Endo, H. Yamamoto, and K. Usami, *J. Phys. Soc. Jpn.* **45**, 1684 (1978).
- ²⁰C. Kittel, *Introduction to Solid State Physics*, 5th ed. (Wiley, New York, 1976), p. 287.
- ²¹H. Raether, in *Excitations of Plasmons and Interband Transitions by Electrons*, edited by G. Höhler (Springer-Verlag, Berlin, 1980).
- ²²Y. Ohno, A. Mineo, and I. Matsubara, *Phys. Rev. B* **40**, 10 262 (1989); Y. Ohno, *ibid.* **46**, 1664 (1992).
- ²³*Handbook of Chemistry and Physics*, edited by R. C. Weast (CRC, Cleveland, 1977).
- ²⁴J. E. Inglesfield, *J. Phys. C* **16**, 403 (1983).
- ²⁵T. Fujikawa, *J. Phys. Soc. Jpn.* **55**, 3244 (1986).